HHS Public Access

Author manuscript

Cleft Palate Craniofac J. Author manuscript; available in PMC 2020 November 05.

Published in final edited form as:

Cleft Palate Craniofac J. 2017 July ; 54(4): 408–422. doi:10.1597/15-120.

Velopharyngeal Structural and Functional Assessment of Speech in Young Children Using Dynamic Magnetic Resonance Imaging

Jamie L Perry, PhD[1] [Associate Professor], David P Kuehn, PhD[2] [Professor Emeritus], Bradley P Sutton, PhD[3] [Associate Professor], Xiangming Fang, PhD[4] [Associate Professor]

[1]3310 Allied Health Sciences, Department of Communication Sciences and Disorders, East Carolina University, Greenville, NC 27834;

[2]Department of Speech and Hearing Science, 901 S. Sixth Street, Champaign, IL 61820; University of Illinois at Urbana-Champaign;

[3]Department of Bioengineering, 1304 West Springfield Avenue, Urbana, IL 61801; University of Illinois at Urbana-Champaign;

[4]2435F Allied Health Sciences, Department of Biostatistics, East Carolina University, Greenville, NC 27834;

Abstract

Objective: The purpose of this study was to demonstrate a novel method for examining the velopharyngeal mechanism using static and dynamic MRI at the sentence level production in young children with normal anatomy. This study examined whether velopharyngeal events occurring in the midsagittal plane are correlated to muscle events occurring along the plane of velopharyngeal closure. Adenoid involvement in velopharyngeal function was also explored.

Methods: A high resolution, T2-weighted turbo-spin-echo 3D anatomical scan was used to acquire static velopharyngeal data and a fast-gradient echo FLASH multi-shot spiral technique (15.8 fps) was used to acquire dynamic data on 11 children between 4–9 years of age.

Results: Changes in velar knee height from rest to the bilabial production was strongly correlated with changes in the velar configuration ($r = .680$, $P = .021$) and levator muscle contraction ($r = .703$, $P = .016$). Velar configuration was highly correlated to levator muscle changes ($r = .685$, $P = .020$). Mean alpha angle during bilabial production was 176 degrees demonstrating subjects achieve velopharyngeal closure at or just below palatal plane. Subjects with a larger adenoid pad used significantly less ($r = -.660$, $P = .027$) levator muscle contraction compared to individuals with smaller adenoids.

Conclusions: This study demonstrates a potentially useful technique in dynamic MRI that does not rely on cyclic repetitions or sustained phonation. This study lends support to the clinical potential of dynamic MRI methods for cleft palate management.

Corresponding Author: Jamie Perry, 3310Q Allied Health Sciences, Department of Communication Sciences and Disorders, East Carolina University, Greenville, NC 27834; perryja@ecu.edu; phone: (252) 744-6144; fax: (252) 744-6104.

Keywords

craniometry; imaging study; levator veli palatini; MRI

Introduction

The most commonly used clinical methods for visualizing the velopharyngeal mechanism are nasendoscopy and multiview videofluoroscopy (Skolnick and Cohn, 1989; Witzel and Stringer, 1990; Sader et al., 1994; Hess et al., 1996). Nasendoscopy is considered invasive and not always well tolerated by young children. Additionally, it is associated with depth distortion cues of the velopharynx (Pigott, 2002). Videofluoroscopy (like computerized tomography and static-view x-ray) uses ionizing radiation and is therefore not recommended for prolonged and repeated use in young children. Neither nasendoscopy nor videofluoroscopy can provide direct visualization of the velopharyngeal muscles. Additionally, these methods may be limited in the viewpoints that can be obtained. Magnetic resonance imaging (MRI) offers an imaging method that is noninvasive, easily repeatable, and allows for views of underlying musculature. There are no dynamic clinical protocols which can visualize the primary velopharyngeal muscles during speech tasks using adequate imaging speeds.

Several studies have demonstrated dynamic speech MRI developments for imaging the vocal tract, lingual movements, and pharyngeal cavity changes during speech (Narayanan et al., 2004; Niebergall et al., 2013; Scott et al., 2014). Dynamic MRI methods of velopharyngeal motions have been reviewed previously (Perry et al., 2014c; Scott et al., 2014) and include Turbo Spin Echo (TSE) “zoom” sequence (Beer et al., 2004), fast spin echo sequences (Yamawaki et al., 1997), fast gradient-echo sequences and echo-planar imaging (Wein et al., 1991; Suto et al., 1993; Gilbert et al., 1998; Anagnostara et al., 2001), fast imaging with steady state precession (TrueFISP) (Atik et al., 2008; Drissi et al., 2011; Scott et al., 2012), and 2D fast low angle shot imaging (FLASH; Sagar and Nimkin, 2015). Methods for speech tasks among studies have been limited to prolonged speech tasks (McGowen et al., 1992; Özgür et al., 2000; Vadodaria et al., 2000; Ha et al., 2007; Atik et al., 2008; Kao et al., 2008; Tian et al., 2010a; Drissi et al., 2011). New imaging methods have been able to achieve speeds of around 20 frames per second (Scott et al., 2012; Sagar and Nimkin, 2015) with more recent developments as high as 100 frames per second (Fu et al., 2015a, 2015b). However, these new technologies have yet to be demonstrated in children. Dynamic MRI investigations among young children have been limited to sustained (2–5 seconds) individual phoneme productions (Tian et al., 2010a, 2010b; Kollara and Perry, 2014; Sagar and Nimkin, 2015). MRI sequences requiring sustained productions lose the co-articulatory effect of sounds and oversimplify the complexity of dynamic speech. Additionally, frame rates less than 10 fps are particularly disadvantageous in the region of the velopharyngeal mechanism where velar elevation may occur in less than 100 ms (Kuehn, 1976).

Studies continue to emphasize the need for a clinical dynamic tool for assessing velopharyngeal structure and muscle function (Atik et al., 2008; Bae et al., 2011a; Kao et al., 2008; Shinagawa et al., 2005; Silver et al., 2011). Fast oblique coronal MR imaging is

particularly beneficial because it allows for assessment of the levator muscle function, which is not possible using traditional imaging methods. Perry et al. (2014c) applied a previously described imaging sequence (Sutton et al., 2009, 2010) to the oblique coronal image plane to obtain dynamic levator muscle data at 15.8 fps among 10 adult males using a gradient echo fast low angle shot (FLASH) multi-shot spiral technique. The primary advantage of these methods is that the MRI techniques do not rely on cyclic repetitions of speech and can be obtained in multiple image planes. These methods, however, have not been examined using a clinically relevant age range in the child population.

Studies have examined lateral-view velopharyngeal function using videofluoroscopy and MRI. These studies have described variations in velar height between subjects (McKerns and Bzoch, 1970). McKerns and Bzoch (1970) proposed that the observed variations between subjects may be due to functional variations in the velar muscles, likely the levator muscle. Kuehn and Moon (1998) used electromyography to provide further support that the levator muscle likely is a significant contributor to the velar morphology and shape during speech. To our knowledge, no studies have demonstrated a method for assessing the effect of levator muscle changes (seen in the oblique coronal image plane) on velar configuration and function (seen in the midsagittal image plane) among children. Combining data from these two image planes provides a powerful means for assessing and understanding the complexities of the three-dimensional velopharynx during a speech gesture.

The purpose of this study was to demonstrate an MRI protocol for obtaining static anatomic data and fast oblique coronal and sagittal MRI data among young children (4–9 years of age) using sentence level stimuli (study AIM I). The second aim of this study used a single phoneme from the sentence stimuli to examine the relationship between velopharyngeal events occurring in the midsagittal plane and levator muscle changes occurring along oblique coronal image plane (study AIM II). Changes in velar configurations during the production of were assessed and discussed relative to the fully relaxed lowered velar position at rest. Lastly, due to likely involvement in the adenoid pad in velopharyngeal closure among the child population, this study examined how midsagittal adenoid size impacts velar, portal, and levator muscle function during the single phoneme stimulus (study AIM III).

Methods

Subjects

In accordance with the Institutional Review Board, 11 healthy subjects between 4–9 years of age (mean, 6.7 years +/− 1.8 years) were recruited to participate in the study. The age range of 4–9 years was selected because it is a common age range in which children with repaired cleft palate who present with hypernasal speech may undergo resonance assessments for consideration of secondary surgery. Studies have demonstrated minimal variations in the velopharyngeal anatomy between children of this age range (Perry et al., 2015). Additionally, Vorperian et al. (2011) suggested a 5-year age span to be an adequate range for comparisons and further cautioned structural comparisons across a decade given the known variations in growth rate and growth trends between males and females. Perry et al. (2015) and Kollara et al. (2015) demonstrated a lack of sexual dimorphism among children between

4–9 years of age. Similarly, for the present study we did not expect sex variations for variables of interest. As seen in Table 1, six children were male and five were female. All subjects were White native English speakers to control for the known racial differences in velopharyngeal structures among children (Kollara et al., 2015; Perry et al., 2015). Subjects reported no history of swallowing, neurological, craniofacial, or musculoskeletal disorders. Subjects reported no history of adenoidectomy or head and neck surgery. Subjects had a mean weight of 25 kg (SD = 6 kg) and height of 132 cm (SD = 10.5 cm). All subjects were judged using a conversational speech sample and a 5-point rating scale using the Americleft protocol (Chapman et al., 2014) performed by a speech-language pathologist with 15 years of experience in resonance evaluations. The 5-point rating scale provided an assessment of overall nasality from normal (rating of 1) to severe hypernasality (rating of 5). Children repeated the sentence stimuli to ensure they did not present with articulation disorders for the targeted sounds. No subjects were enrolled in speech or language therapy at the time of the study.

Magnetic Resonance Imaging

We utilized a previously published child-friendly protocol (Kollara and Perry, 2014) which includes the use of printed material for the child subjects (such as coloring books) and caregiver (information regarding the scanning process). On the day of the MRI, subjects listened to MRI noises through headsets outside of the MRI scanning room. Cushions, an elastic strap, and foam wedges were used to secure the head and reduce the overall motion while in the scanner. A blanket was used to swaddle the subject's arms and legs to limit overall body motion. Blankets were stored in an electric warming container. Because the MRI scanning room was cold, child subjects were accepting of the blanket. During static image acquisition, children were provided the option to watch a movie to maintain a fixed eye gaze and thus reduce head motion. Children were given a panic button that could be pressed at any time to immediately terminate the study.

Each subject was positioned similarly in the head coil to control for variations in head flexion and extension between subjects. Specifically, the nose tip was positioned at the same point on the head coil and the localizer MRI sequence was viewed to determine if the child had too much head flexion or extension. In cases where excessive head flexion or extension was noted, the child was repositioned within the head coil. The degree of head flexion and extension was further evaluated using the MRI data to ensure there was minimal difference between subjects in the position of their head in the coil. This was examined by measuring the angle created between a vertical line passing along the anterior edge of the C2-C3 cervical vertebrae and a line connecting the posterior tip of the spinous process of the first cervical vertebra and the tuberculum sella across all subjects (Figure 1). Values indicated less than 16.3 degrees of variation in the head flexion/extension between subjects. Previous research has demonstrated that less than 20 degrees of extension or flexion has no effect on upper airway dimensions (Jan et al., 1994).

Subjects were scanned in the supine position using a Siemens 3 Tesla Trio MRI scanner (Erlangen, Germany) and a 12-channel Siemens Trio head coil. Images were obtained at rest breathing and during speech production. During the static rest images, each subject was

instructed to breathe through their nose with their mouth closed. The velum was in a relaxed and lowered position. Table 2 displays MRI parameters. A high resolution, T2-weighted turbo-spin-echo three dimensional (3D) anatomical scan called Sampling Perfection with Application optimized Contrasts using different flip angle Evolution (SPACE) was used to acquire a large field of view covering the oropharyngeal anatomy ($25.6 \times 19.2 \times 15.5$ cm^3) with .8 mm isotropic resolution, 2500 ms repetition time, 268 ms (with echo train length of 171), .8 mm slice thickness, and with an acquisition time of slightly less than 5 minutes (4:52).

Dynamic images were obtained using a gradient echo fast low angle shot (FLASH) multi-shot spiral technique to serially acquire images for 50.5 seconds for 799 native frame rate (15.8 fps) or 1515 sliding window images at 30 fps (Table 2). This sequence has been described previously (Sutton et al., 2009, 2010) and applied to an adult population with normal anatomy (Perry et al., 2014a, 2014b). The sliding window reconstruction is performed by deciding the desired time points for reconstruction at 30 fps and using the k-space data that was acquired closest in time to each time point. A time-efficient acquisition of a six-shot spiral pulse sequence with an alternating echo time (TE) between 1.3 and 1.8 ms was used to allow dynamic estimation and correction of the magnetic field map. Images were obtained at $1.87 \times 1.875 \times 8$ mm^3 spatial resolution. Multiple saturation bands were placed around regions of higher fat concentration (cheeks) to suppress the high intensity signal from these regions while also limiting the field of view that must be measured. These methods provide a higher image quality, improved signal-to-noise ratio, and increase the overall rate of image acquisition. Fast frame rates are achieved through an optimized acquisition strategy coupled with an image reconstruction method that corrects for effects caused by imperfections in the magnetic field in the oropharyngeal region (Sutton et al., 2009, 2010). The imaging quality and contrast variation evident in Figures 2 and 3 are related to the differences in static (used for measuring rest condition) and dynamic imaging protocols (used to measure single production selected from sentence stimuli).

Previous investigations utilized this dynamic sequence on adult subjects during the production of /ansa/ (Perry et al., 2014b). For the present study, a sentence was used to elicit a more natural speech production from the child subjects and to demonstrate a method for rapid MRI during speech (study AIM I). The sentence, “pick up a puppy,” was selected because it is void of nasal sounds and has high pressure sound productions. We also aimed to use a stimulus that may be similar to sentence stimuli used in resonance assessments done by a speech language pathologist. For study AIMS II and III, preliminary analyses of the single phoneme in the word “up” in the stimulus phrase “pick up a puppy” was analyzed. In addition to serving as preliminary analyses, a single phoneme was analyzed to limit statistical comparisons given the small sample size. The in the word “up” was chosen to avoid sentence starting and ending effects which would be expected to be more variable compared to a medially-positioned sound production. Additionally, only one production was used to facilitate participant compliance and to avoid disinterest among the child subjects. Subjects were trained and practiced the speech productions prior to the imaging session while simultaneously listening to pre-recorded MRI scanning noises over headphones. This was done to simulate the testing environment inside the magnet and to assess the child’s accuracy in producing the target speech sample.

Subjects were instructed to repeat the sentence “pick up a puppy” at the start of the loud scanning noise while in the MRI magnet. The investigator in the scanning room provided tactile cues for pacing the repetitions by tapping the child’s leg during the scan while listening and being paced to a metronome beat played over headphones. Speech was produced at a rate of 2.5 seconds per sentence. Although the MRI methods do not require rate to be controlled given the non-cyclic nature of the data acquisition, we chose to pace the productions to avoid variations in velar function caused by speech rate. Simultaneous audio recordings were conducted using an Optoacoustic fiber optic MRI-compatible microphone (Optoacoustics, FOMRI-III, 2009), which provides automatic noise cancellation and audio filtering of acoustic speech signals. The microphone and headphones allowed the examiner in the control room to evaluate each production in real-time to ensure accurate production of the target speech stimuli. If the child did not produce the sentences accurately or could not keep a consistent pace, the sequence was repeated. The sequence was repeated only once for one of the 11 subjects for incorrect production of the sentence. Fast dynamic midsagittal data was obtained first followed by oblique coronal fast dynamic data. These data (oblique coronal and sagittal speech images) were not obtained simultaneously due to the desire to keep the acquisition frame rate high for each sample and to avoid interactions of the two imaging slice locations. Future work will be able to leverage developing technologies to image 3D at sufficient frame rates (Fu et al., 2015).

Dynamic images were acquired on the MRI scanner at a native frame rate of 15.8 fps and image reconstruction was performed off-line using an output time-driven sliding window process which takes approximately 2 hours per subject to compute. The reconstruction procedure was an iterative image estimation that takes into account the dynamically measured magnetic field maps to correct for image distortions (Sutton, 2003). The sliding window reconstruction process minimizes temporal blurring by reducing redundant information in adjacent time points (Sutton et al., 2009, 2010). This process uses 30 fps as the output image rate by gathering k-space data closest to the desired time point. The result is a minimal amount of interpolation across time. Alternatively, the images in the native frame rate (15.8 fps) could be interpolated to the desired output rate, but this would result in significant blurring of information across time. Acquisition simulation software provided by the vendor of the MRI scanner provides timing data used to align audio speech recordings with the dynamic images. This software allows for accurate simulations of sequence timing using the exact acquisition protocol, giving information about the actual time location of data acquisition events with 10 μs accuracy.

Image Analyses

Image processing methods were consistent with previously reported methods (Perry et al., 2011). Images were transferred into Amira 4 Visualization Volume Modeling software (Visage Imaging GmbH, Berlin, Germany). This program has a built-in native Digital Imaging and Communication in Medicine (DICOM) support program which enables data to preserve original geometry. Dynamic MRI data were exported as an image sequence using Adobe After Effects (Adobe, CS5.5, v10.5). The exported audio signal was analyzed using Praat (Praat, v5.3.53) to identify the consonant production of in the word “up”. Noise cancelling and audio filtering features of the Optoacoustic microphone provide delineation

of the audio signal from the MRI scanner noise. Specifically, the microphone system filters and removes the noise from the acoustic signal enabling a clear representation of the acoustic features in the plosive phoneme. The image frame for the corresponding acoustic location was noted and used to index the exported image sequence. Inspection of the imaging data ensured accuracy of identified acoustic features. For example, the stop plosive production of the was identified by the acoustic burst noted on the spectrogram and confirmed by noting bilabial articulatory positon. In all cases, the acoustic data (spectral analyses) were accurate and reliable in identifying the plosive production. Using acoustic data instead of visual inspection of images proved to be a more accurate and consistent method for identifying the image location for the target phonemes.

Sagittal images were used to obtain the ABC and alpha angle, shown in Figure 2. The ABC angle described by McKerns and Bzoch (1970) was used to represent the overall configuration and orientation of the velum in the nasopharynx. Specifically, it was formed by lines from the posterior nasal spine (point A) to the superior most point of velar contact (point B) and from point B to the inferior tip of the uvula (point C). The ABC angle becomes more acute as the velar knee (point B) gets higher and/or when the uvular tip (point C) curves anteriorly away from the posterior pharyngeal wall (Figure 2). The alpha angle, as described by Lipira et al. (2011), represents the height of the velar knee relative to the palatal plane and can be described by connecting points from the anterior nasal spine, posterior nasal spine, to the velar knee (Figure 3). As the velar knee elevates, the alpha angle increases (Figure 3). An alpha angle of 180 degrees during bilabial production indicates the velar knee to pharyngeal wall contact is directly in line with the palatal plane.

The mean (right and left) levator muscle length was measured as the distance from the origin at the base of the skull to the midline of the velum (Figure 4). The angle of the levator muscle was defined as the angle created at the base of the skull as the muscle converges towards the velum (Figure 4). The ABC angle, alpha angle, and levator muscle (length and angle of origin) measures were obtained at rest from the 3D static MRI data and during the production from the dynamic MRI data. Rest images were obtained from the 3D static MRI data because during speech tasks children most often showed an anticipatory position (e.g., velum slightly elevated) for speech articulators, as opposed to a fully rest position (e.g., velum lying on the base of the tongue). Because children are known to often have an adenoid-to-velar closure pattern, we examined adenoid thickness and distance from the velar knee to the posterior pharyngeal wall from a single midsagittal static image at rest. These measures were then used to examine how adenoid involvement relates to velar and muscle function. Adenoid thickness was measured by first drawing a reference line through palatal plane. A second reference line was drawn along the posterior pharyngeal wall. The intersection of these two lines served as the posterior margin of the adenoid tissue. As seen in Figure 5, the midline adenoid thickness was determined as the distance from the nasopharyngeal margin (anterior margin open to the nasopharynx) to the intersection of these lines. Figure 5 provides a comparison of a child with adenoid tissue to that of a child without adenoid tissue involvement.

Statistical Analysis

All statistical analyses were conducted in IBM SPSS Version 21.0 (IBM Corporation, Armonk, NY). Measures were compared between rest and bilabial production using matched pairs t-tests. Scatterplots showed the relationships between variables were generally linear, thus Pearson correlations were used. Pearson correlations were used to determine if events occurring in the sagittal image plane (velar movement) are correlated with levator muscle length changes occurring in the oblique coronal image plane. Correlation analyses were also used to determine if the velar and levator muscle movement is correlated to adenoid size or velar to adenoid distance.

Reliability

A primary rater (speech pathologist with over 15 years of experience in MRI research) and secondary rater (graduate speech pathology student with 4 years of experience in MRI research) randomly selected and re-measured data from five subjects five months after the initial measures were obtained. Anatomical static images at rest were scaled and overlaid onto the dynamic rest image at the start of the speech segment to ensure reliable identification of the major landmarks used for dynamic MRI data including anterior nasal spine, posterior nasal spine, velar knee, and uvular tip for sagittal images. The amount of scaling was determined determining the percent difference between static and dynamic voxel size in the plane of interest. A computer graphics program was used scale the serially exported image sequences using the percent difference. Oblique coronal images were aligned by overlapping the petrous bony segment of the temporal bone, which is a distinctive feature on the oblique coronal images. Reliability of the measures from the plosive phoneme were assessed using inter- and intra-rater reliability. A training period was conducted between raters using two subjects from our adult MRI dynamic data which used the same imaging parameters.

Inter-rater and intra-rater reliability measures (using a .05 level of significance) were obtained using the Pearson product moment correlation. As seen in Table 3, reliability ratings were high. There was no significant difference ($p > .05$) between observers or within the primary observer using a paired samples t-test. Interclass correlation using a two-way mixed model with 95% confidence interval was used to examine the consistency of measures between raters and within the primary rater. Values for interclass correlations ranged from .78 to .98 for inter-rater reliability and .65 to .98 for intra-rater reliability.

Results

Fast Oblique Coronal and Sagittal MRI Protocol for Young Children:

The first aim of this study was to demonstrate an MRI protocol for obtaining static anatomic data and fast oblique coronal and sagittal MRI data among young children (4–9 years of age) using sentence level stimuli. All subjects completed the MRI tasks within the protocol. As seen in Figure 6, the study MRI protocol provides high image resolution (.8 mm in plane resolution) of patient anatomy at rest in multiple viewpoints. Images are acquired from a single acquisition. Similar to lateral-view videofluoroscopy and static lateral-view x-ray, measures of velar length, velopharyngeal depth, and craniometric measures can be obtained.

The original DICOM format native to MRI serves to preserve the original geometry and shape configurations. As a result, the aspect ratio is known and measures can be reliably obtained. However, unlike lateral-view videofluoroscopy and static lateral-view x-ray, MR images display in-plane anatomy and are not projected onto overlying anatomy. The most significant advantage of MRI is the ability to visualize velopharyngeal muscles. Figure 7 displays the levator muscle, musculus uvulae, and the relationship to velar segments of the palatoglossus muscle. Three- dimensional imaging allows for any image plane to be visualized. For example, Figure 7 demonstrates the relationship between the levator and tensor veli palatini muscle.

This study also demonstrates the use of a novel dynamic MRI protocol for use in young children with speech production at the sentence level. Images are obtained with high imaging speeds and can be obtained using natural speech because methods do not rely on speech to be cyclic. The trade-off for high-speed imaging is image quality. As evident in Figures 2 and 3 (comparing rest to dynamic condition), image quality of the dynamic images is not as good as the static 3D images. Motion was a factor in the present study. Although the scanning sequence only requires the child to say the sentence one time, a child may move between the time he/she is placed inside the scanner and the dynamic data are obtained. Due to the single-slice nature of the dynamic imaging used in this study, an incorrect slice location could result if a child moved between the structural scan, which was used to identify the orientation and position of the muscles, and the dynamic scan. Motion is also a problem for lengthy static structural scans which require the child to remain still for large data sampling. We obtained two static structural scans in our protocol in order to have a back-up image if the child moved. However, we did not observe a loss of image quality on either structural scan for any of the subjects.

Dynamic imaging sequences can potentially suffer from magnetic susceptibility artifacts due to the large magnetic susceptibility differences between tissue and air in the dynamically changing oral cavity. We countered potential image distortion artifacts in the dynamic imaging by integrating a dynamic magnetic field map measurement into the acquisition and reconstruction. Images were acquired with alternating echo times (1.3 ms and 1.8 ms) in order to sample the susceptibility-induced magnetic field changes. These dynamic field maps were incorporated into the reconstruction for each time point, see Sutton et al. (2009, 2010) for a full description of the dynamic image acquisition and reconstruction process along with comparisons of the impact of these choices. Magnetic susceptibility can still impact the images despite the susceptibility-corrected image reconstruction by causing shifts in the frequency of structures around air/tissue interfaces, resulting in certain structures being accidentally saturated by our spatially selective saturation bands. This would appear as the velum disappearing when it was raised, for example. In order to counter this effect, we ensured that we placed our spatial saturation bands far enough away from the velum such that the frequency shifts would not cause it to be saturated. This was examined in previous studies on adults, but none of the children in the current study suffered from this effect.

Correlating Velar and Levator Muscle Events during Production:

The second aim of this study used a single phoneme from the sentence stimuli to provide preliminary investigations of the relationship between velopharyngeal events occurring in the midsagittal plane and levator muscle changes occurring along oblique coronal image plane. Changes in velar configurations during the production of were assessed relative to the fully relaxed lowered rest velar position. The values for rest position are intended to provide a reference for the amount of movement for production compared to a non-speech position. As seen in Table 4, the mean ABC angle at rest was 142 degrees (SD = 7 degrees) and 80 degrees (SD = 6 degrees) during the bilabial production. Mean alpha angle at rest was 155 degrees (SD = 10 degrees) and 176 degrees (SD = 4 degrees) during the bilabial production. This demonstrates that during the bilabial production, child subjects achieve velopharyngeal closure at (180 degrees) or just below (less than 180 degrees) the palatal plane. Mean muscle length at rest was 39.5 mm (SD = 2.9 mm) and 30.3 mm (SD = 4.4 mm) during the bilabial production. The mean angle of levator muscle at the muscle origin was 56 degrees (SD = 2 degrees) for rest and 46 degrees (SD = 3 degrees) for the bilabial production. Velar (ABC and alpha angles) and muscle (length and angle of origin) parameters at rest were significantly different from measures during the speech condition as determined using paired sample t-tests ($P < .001$ for all pairs; Table 4).

Changes in velar knee height (alpha angle) from rest to the bilabial production was strongly correlated ($r = .680$, $P = .021$; Table 5) with changes in the velar configuration (ABC angle). This means as the velar knee elevates from rest condition to the bilabial production, the flexion or angle of the velum becomes more pronounced (i.e., more acute). Subjects with greater velar height (more acute alpha angle) during the bilabial production demonstrated greater flexion of the velum. Changes in the alpha angle from rest to the bilabial production was strongly correlated ($r = .703$, $P = .016$; Table 5) to changes in the length of the levator muscle. As expected, as the levator muscle shortened, the velar knee elevated. Subjects with greater muscle shortening demonstrated greater velar height. Shortening of the levator muscle was also correlated ($r = .685$, $P = .020$; Table 5) to velar configuration (ABC angle). Specifically, greater muscle contraction resulted in a greater degree of flexion of the velar body. Greater levator muscle contraction resulted in a greater change (i.e., more acute) angle of origin ($r = .814$, $P = .002$). As expected, as the muscle contracts, the velum is elevated causing the angle of muscle origin to become more acute. Individuals with greater levator muscle contraction during the bilabial production displayed a more acute angle of muscle origin.

Impact of Adenoid Size on Velopharyngeal Function:

The third aim of this study was to examine how midsagittal adenoid size impacts velar, portal, and levator muscle function during the single phoneme stimuli. Midline adenoid thickness and distance from the velum to adenoid tissue (or pharyngeal wall when devoid of adenoid tissue) was used to examine the relationship between velar, portal, and levator muscle functions between rest and the bilabial production (representing the change between positions). Ten of the 11 subjects displayed velar to adenoid contact and 1 subject (Subject 7) displayed velar to posterior pharyngeal wall contact for velopharyngeal closure during the bilabial production. As seen in Table 4, mean adenoid thickness was 4.7 mm (SD = 2.5 mm)

and the mean distance from the velar knee to the adenoid (or pharyngeal wall in two subjects) was 8.3 mm (SD = 1.9). It was hypothesized that individuals with larger adenoids would show a decrease in flexion (ABC angle), velar height (alpha angle), and less levator muscle contraction. Velar flexion (ABC angle) and velar knee height (Alpha angle) were not significantly correlated to adenoid thickness (Table 6). However, it was observed that subjects with a larger adenoid pad displayed significantly less levator muscle contraction (r = −.660, P = .027; Table 5) and less change in the muscle angle of origins (r = −.770, P = .006). As expected, if the adenoid pad was larger, subjects did not require as much muscle contraction (shortening) and therefore displayed less change in the angle of origins compared to those with smaller adenoid tissue. Adenoid size was not significantly correlated with velar to adenoid distance (r = −.498, P = .119). The size of the velopharyngeal port did not correlate to any of the variables.

Discussion

Fast Oblique Coronal and Sagittal MRI Protocol for Young Children:

MRI offers many advantages in speech assessments for young children. As previously mentioned, the most notable advantages of MRI over traditional imaging tools are that it does not expose the child to radiation (compared to videofluoroscopy and static-view x-ray), it is non-invasive (compared to nasendoscopy), and muscles can be visualized directly. MRI is an easily reproducible and repeatable tool for clinical evaluation and it is the only method for viewing the velopharyngeal muscles at rest and during functional speech tasks. Unlike traditional imaging methods, MRI is obtained in the supine position. However, previous studies have not demonstrated a significant difference in velopharyngeal positioning and functions between the upright and supine positions (Perry, 2011; Kollara and Perry, 2014). Studies assessing other areas of the speech system have also observed minimal to no gravitational influence (Yildrim et al., 1991; Traser et al., 2013). Bae et al. (2014) further demonstrated structural positioning to be more closely dependent on the target stimuli and adjacent sounds, than patient orientation in the scanner. These data provide support for using supine imaging speech data of the velopharyngeal mechanism for decisions about the mechanisms of speech.

MRI methods in the current study provide a promising advancement in the development of a clinically useful MRI protocol for cleft palate care. An optimal imaging protocol for use in children with cleft palate would provide for volumetric assessment of the anatomy as well as a functional assessment that can be obtained under a minute and that provides immediate data analyses and interpretation (Perry et al., 2014c). Additionally, methods should allow for natural speech samples at the sentence level as opposed to prolonged speech sounds, which most MRI studies of velopharyngeal function to date have utilized (McGowen et al., 1992; Özgür et al., 2000; Vadodaria et al., 2000; Ha et al., 2007; Atik et al., 2008; Kao et al., 2008; Tian et al., 2010a; Drissi et al., 2011). The current study (AIM I) demonstrates the use of sentence level production during a dynamic image acquisition. Variations in muscle function within a sentence cannot be visualized through dynamic MRI techniques that rely on gated acquisition procedures (Kane et al., 2002; Shinagawa et al., 2005). Gated procedures are ideal for cyclic processes with a high degree of repetition across each cycle, such as in

cardiac imaging. These methods are not suitable for analysis of temporal variations in speech. MRI methods used for dynamic assessment in the present study represent serial acquisition at high imaging speeds of 15.8 fps and do not rely on cyclic repetitions for speech. MRI protocols in children should also include image planes for assessing velar function (i.e., axial and midsagittal planes) and for assessing muscle function (i.e., oblique coronal plane). Dynamic MRI studies thus far have presented data in the midsagittal and/or axial image planes (Kane et al., 2002; Bae et al., 2011a; Drissi et al., 2011). However, these two image planes do not display details of the velopharyngeal muscles. In such, these images do not capitalize on the major benefit of MRI, i.e., the ability to image muscle function.

Further developments are needed to translate research MRI scanning protocols to clinical scanners and clinical workflow. The normal process of translation of MRI developments begins by creating new research MRI sequences and assessing the outcomes on clinically relevant populations. The current dynamic methods use a non-Cartesian acquisition process which is not found on clinical scanners and require off-line image reconstruction. Scott et al. (2012) demonstrated a method using a Cartesian acquisition process which allows for on-scanner reconstruction and is more readily accessible on clinical scanners. However, these methods acquire images at a slower frame rate. We have begun to translate our dynamic protocols to clinical MRI scanners to assess the feasibility, repeatability, validity, and reliability. In addition to the translation of the acquisition sequence, research is needed to automate the interpretation of MRI data for on-demand assessment of speech function. Most dynamic MRI research methods, such as in the present study, require off-line processing to create a MRI movie. This results in a delay in the clinical process. Technological advancements are needed to create a more rapid and automated method for visualizing dynamic MRI data to apply research imaging methods to clinical practice. Through collaboration with those involved in resonance assessments and treatment planning (i.e., surgeons and speech language pathologists), further research should determine which variables and data outputs are of clinical relevance and provide insight into the treatment planning process.

Correlating Velar and Levator Muscle Events during Production:

Although many studies have demonstrated the potential utility of MRI as an additional clinical tool in cleft palate care, to our knowledge, no studies have used MRI to correlate changes in velar configuration with changes in muscle function. Research related to velar timing, velar function, and velar configuration have been thoroughly documented using techniques such as cine radiography, lateral-view x-ray, and videofluoroscopy. A significant advantage of MRI is the ability to correlate movements that occur in multiple image planes in order to gain understanding of the complex nature of the velopharyngeal mechanism through muscle imaging.

Findings from the present study suggest that velar configuration and movement are highly correlated with levator muscle activity (AIM II) in children with normal anatomy. Greater levator muscle contraction resulted in greater velar height, increased flexion of the velar body, and a decrease in the angle of levator muscle origin. Across subjects, the levator

muscle reduced in length by 22% from rest position to the plosive production. Ettema et al. (2002) observed a 19% reduction from rest to a fricative production among adult participants. This similarity between child and adult data may suggest a constant percentage of contraction regardless of age or size of the structures, which might have important implications with regard to speech motor control. Tian et al. (2010a) demonstrated a range between 8–10% levator muscle shortening across two vowels, a nasal, and a Chinese voiced alveolar affricate among children. This difference between studies is likely due to the variation of phonemes used between the studies, i.e., a high pressure consonant in the present study compared to a mean value obtained from two vowels, a nasal, and a Chinese voiced alveolar affricate.

Tian et al. (2010a) demonstrated variations in velar function during sustained speech tasks among children with noncleft anatomy compared to those with repaired cleft palate and velopharyngeal inadequacy. Children with normal anatomy and normal resonance showed significantly greater velar height when compared to those with hypernasal speech. Children with velopharyngeal inadequacy further displayed almost no velar stretch during sustained phonation. However, the levator muscle shortened a similar degree (ranging from 8–10%) among the three study groups, i.e., noncleft controls, repaired cleft and normal resonance, and repaired cleft with hypernasality. The authors hypothesized that these findings might suggest that velopharyngeal inadequacy is primarily caused by rigidity of the velum. The authors suggested that abnormal levator muscle function likely does not explain the presence of hypernasality among the study groups. It was suggested that rigidity of the velum may be due to scar tissue restricting the palatoglossus and palatapharyngeus muscle to stretch during velar elevation. Results from the present study demonstrate velar function and velar shape are highly related to levator muscle contraction in children with normal anatomy. It is not clear how primary cleft palate surgery impacts the function of the velopharyngeal muscles and structures. It is hypothesized that different scar patterns on the mucosal layers and varied muscle dissection methods may result in different outcomes for velar stretch and movement. However, this area of research is unrepresented in the literature.

Future MRI developments are needed to explore the use of 3D dynamic MRI acquisition sequences (Fu et al., 2015a; Fu et al., 2015b) among the child population. The primary benefit of 3D MRI methods is the ability to re-slice the data to view a single production for multiple anatomic viewpoints during a speech event. Because the present study used 2D dynamic acquisition, children were required to produce the target stimuli twice to sample along two planes (sagittal and oblique coronal). In such, correlating the two events should be done with caution due to the known within speaker variability between events. The use of 3D MRI sequences overcomes this limitation. Our laboratory has begun exploring these methods at frames rates of 100+ fps (Fu et al., 2015a; Fu et al., 2015b).

Impact of Adenoid Size on Velopharyngeal Function:

Isberg et al. (1993) observed enlarged adenoids to be more common in children with repaired cleft palate who have velopharyngeal competence compared to those who had velopharyngeal incompetence. This suggests that adenoid size may have an impact on velopharyngeal function. Findings among children without cleft palate, however, do not

support this functional relationship. Williams et al. (1992) observed that the size of the adenoids has little to no effect on whether a child (noncleft) was at risk of developing nasality post adenotonsillectomy. Nasopharyngeal airway size was more related to the risk of developing nasality than was adenoid volume. In the present study, we anticipated an inverse relationship between adenoid size and nasopharyngeal volume. Specifically, we expected children with larger adenoids would have a smaller nasopharyngeal depth. However, our findings did not show this relationship. It is well established that children generally display a velar to adenoid velopharyngeal closure pattern preadolescence, however, the effect of the relative size of the adenoids on velopharyngeal function is less understood. Additionally, management of adenoid tissue in the cleft population, particularly in children being considered for pharyngoplasty, is an area of less agreement between cleft surgical teams. Nasopharyngeal depth is likely a more important clinical measure than adenoid volume. However, given that adenoids contribute to nasopharyngeal depth, imaging methods which allow for measures of adenoid volume, such as MRI, may provide insights that are not afforded using traditional methods such as nasopharyngoscopy.

Future studies are needed to explore the interaction of adenoids, nasopharyngeal configurations, and muscle variations on the shape and motions of the velum during speech in normal and abnormal anatomy. These investigations should include additional velopharyngeal muscles such as the musculus uvulae, palatoglossus, palatopharyngeus, and superior pharyngeal constrictors. This study demonstrates a method that can be used to examine how multiple muscles contribute to the overall velar position, configuration, and type of closure pattern. Interpretation of data from this study may be limited because this study did not examine the impact of variables such as velopharyngeal structural size and closure patterns on outcomes. Our laboratory is currently investigating additional muscle and velar variables in child speakers with normal and cleft palate anatomy to explore the differences between groups. It is expected these data combined with finite element modeling (Berry et al. 1999; Inouye et al., 2015) will provide insight into which muscle and velar variables are likely to contribute to abnormal resonance.

Study Limitations:

Despite advances in dynamic MRI, there are limitations that need to be addressed prior to clinical application. In addition to motion artifacts, MRI may not be a suitable imaging option for individuals undergoing orthodontic treatment (Elison et al., 2006; Görgülü et al., 2014; Wylezinska et al., 2015). Similar to other clinical imaging methods, MRI may be more challenging for difficult clinical cases such as patients with syndromes or cognitive deficits. The noise generated from the scanner is another limitation of MRI in the pediatric population (Price et al., 2001). In the present study, we used earplugs, headphones, and played music (during non-speech tasks) for the child to reduce the loud noise from the scanner. Additionally, loud noise can interfere with the communication between the patient in the MRI scanner and the examiners in the adjacent room. Analyses of dynamic imaging is particularly challenging because of the time-intensive nature of manually measuring hundreds of sequential images. Assessing only one phoneme, plosive production, is a noted limitation of the present study. Specifically, using a comparison between rest position and a single production during a sentence production provides limited insights into the true

dynamic capabilities of the velopharyngeal portal. Future research is needed to develop automatic methods for data analyses to improve the ability to interpret large volumes of data, such as in the present study.

Conclusion

This study demonstrates a novel MRI protocol for assessing velopharyngeal structure and function in a young child population (4–9 years of age) using sentence level production and increased frame rates compared to the current dynamic MRI literature. Results from this study provide comparisons between velar events and levator muscle function in normal anatomy. Additionally, this study observed that adenoid size was not related to the velar configuration or the velopharyngeal portal distance. However, adenoid size does appear to be related to the amount of levator muscle contraction.

Acknowledgments

This study was made possible by grant number 1R03DC009676-01A1 from the National Institute on Deafness and Other Communicative Disorders. Its contents are solely the responsibility of the authors and do not necessarily represent the official views of the National Institutes of Health.

References

Anagnostara A, Stoeckli S, Weber OM, Kollias MD. Evaluation of the anatomical and functional properties of deglutition with various kinetic high-speed MRI sequences. J Magn Reson Imaging. 2001;14:194–199. [PubMed: 11477680]

Atik B, Bekerecioglu M, Tan O, Etlik O, Davran R, Arslan H. Evaluation of dynamic magnetic resonance imaging in assessing velopharyngeal insufficiency during phonation. J Craniofac Surg. 2008;19(3):566–572. [PubMed: 18520366]

Bae Y, Kuehn DP, Conway CA, Sutton BP. Real-time magnetic resonance imaging of velopharyngeal activities with simultaneous speech recordings. Cleft Palate Craniofac J. 2011a;48(6):695–707. [PubMed: 21214321]

Bae Y, Kuehn DP, Sutton BP, Conway CA, Perry JL. Three-dimensional magnetic resonance imaging of velopharyngeal structures. J Speech Lang Hear Res. 2011b;54(6):1538–1545. [PubMed: 22052285]

Bae Y, Perry J, Kuehn D. Videofluoroscopic investigation of body position on articulatory positioning. J Speech Lang Hear Res. 2014;57(4):1135–1147. [PubMed: 24167231]

Beer AJ, Hellerhoff P, Zimmermann A, Mady K, Sader R, Rummeny EJ, Hannig C. Dynamic near-real-time magnetic resonance imaging for analyzing the velopharyngeal closure in comparison with videofluoroscopy. J Magn Reson Imaging. 2004;20:791–797. [PubMed: 15503349]

Berry DA, Moon JB, Kuehn DP. A finite element model of the soft palate. Cleft Palate Craniofac J. 1999;36(3):217–223. [PubMed: 10342609]

Chapman KL, Baylis A, Trost-Cardamone J, Cordero KN, Dixon A, Dobbelsteyn C, Thurmes A, Wilson K, Harding-Bell A, Sweeney T, Stoddard G, Sell D. The Americleft speech project: a training and reliability study. Cleft Palate Craniofac J. 2014, in press.

Drissi C, Mitrofanoff M, Talandier C, Falip C, Le Couls V, Adamsbaum C. Feasibility of dynamic MRI for evaluating velopharyngeal insufficiency in children. Eur Radiol. 2011;21(7):1462–1469. [PubMed: 21287177]

Elison MJ, Leggitt LV, Thomson M, Oyoyo U, Wycliffe DN. Impact of orthodontic appliances on the quality of craniofacial anatomical magnetic resonance imaging and real-time speech imaging. Am J Orthod Dentofacial Orthop. 2008;134:563–572. [PubMed: 18929275]

Fu M, Barlaz MS, Holtrop JL, Perry JL, Kuehn DP, Shosted RK, Liang Z, Sutton BP. High-resolution full-vocal-tract 3D dynamic speech imaging. Magn Reson Med. 2015a, under review

Fu M, Bo Z, Shosted RK, Perry JL, Kuehn DP, Liang Z, Sutton BP. High-resolution dynamic speech imaging with joint low-rank and sparsity constraints. Magn Reson Med. 2015b;73(5):1820–1832. [PubMed: 24912452]

Gilbert RJ, Daftary S, Campbell TA, Weisskoff RM. Patterns of lingual tissue deformation associated with bolus containment and propulsion during deglutition as determined by echo-planar MRI. J Magn Reson Imaging. 1998;8:554–560. [PubMed: 9626868]

Görgülü S, S Ayyıldız S, K Kamburoğlu K, Gökçe S, Ozen T. Effect of orthodontic brackets and different wires on radiofrequency heating and magnetic field interactions during 3-T MRI. Dentomaxillofac Radiol. 2014;43(2):20130356. [PubMed: 24257741]

Ha S, Kuehn DP, Cohen M, Alperin N. Magnetic resonance imaging of the levator veli palatini muscle in speakers with a repaired cleft palate. Cleft Palate Craniofac J. 2007;44(5):494–505. [PubMed: 17760495]

Hess U, Hannig C, Sader R, Cavallaro A, Wuttge-Hannig A, Zeilhofer H. Evaluation of velopharyngeal closure in preoperative planning of maxillary advancement. Rontgenpraxis. 1996;49:25–26. [PubMed: 8851543]

Inouye JM, Pelland CM Lin KY, Borowitz KC, Blemker SS. A Computational Model of Velopharyngeal Closure for Simulating Cleft Palate Repair. J Craniofac Surg. 2015;26(3):658–662. [PubMed: 25974769]

Isberg A, Ren YF, Henningsson G, McWilliam J. Facial growth after pharyngeal flap surgery in cleft palate patients: a five year longitudinal study. Scan J Plast Reconstr Surg Hand Surg. 1993;27:119–126.

Jan MA, Marshall I, Douglas NJ. Effect of posture on upper airway dimensions in normal human. Am J Respir Crit Care Med. 1994;149:145–148. [PubMed: 8111573]

Kane AA, Butman JA, Mullick R, Skopec M, Choyke P. A new method for the study of velopharyngeal function using gated magnetic resonance imaging. Plast Reconstr Surg. 2002;109(2):472–481. [PubMed: 11818823]

Kao DS, Soltysik DA, Hyde JS, Gosain AK. Magnetic resonance imaging as an aid in dynamic assessment of the velopharyngeal mechanism in children. Plast Reconstr Surg. 2008;122(2):572–577. [PubMed: 18626376]

Kuehn DP. A cineradiographic investigation of velar movement variables in two normal. Cleft Palate Craniofac J. 1976;13:88–103.

Kuehn DP, Moon JB. Velopharyngeal closure force and levator veli palatini activation levels in varying phonetic contexts. J Speech Lang Hear Res. 1998;41:51–62. [PubMed: 9493733]

Kollara L, Perry JL. Effects of gravity on the velopharyngeal structures in children using upright magnetic resonance imaging. Cleft Palate Craniofac J. 2014, 51(6):669–676. [PubMed: 24060001]

Kollara L, Perry JL, Hudson S. Racial Variations in Velopharyngeal and craniometric morphology in children: an imaging study. J Speech Lang Hear Res. 2015, in press.

Lipira AB, Grames LM, Molter D, Govier D, Kane AA, Woo AS. Videofluoroscopic and nasendoscopic correlates of speech in velopharyngeal dysfunction. Cleft Palate Craniofac J. 2011;48(5):550–560. [PubMed: 20815707]

McGowen J, Hatabu H, Yousem D, Randall P, Kressel H. Evaluation of soft palate function with MRI: application to the cleft palate patient. J Compt Assist Tomogr. 1992;16:877–882.

McKerns D, Bzoch KR. Variations in velopharyngeal valving: The factor of sex. Cleft Palate Craniofac J. 1970;7:652–662.

Narayanan S, Nayak K, Lee S, Sethy A, Byrd D. An approach to real-time magnetic resonance imaging for speech production. J Acoust Soc Am. 2004;115:1771–1776. [PubMed: 15101655]

Niebergall A, Zhang S, Kunay E, Keydana G, Job M, Uecker M, Frahm J. Real-time MRI of speaking at a resolution of 33ms: undersampled radial FLASH with nonlinear inverse reconstruction. Magn Reson Med. 2013;69(2):477–85. [PubMed: 22498911]

Özgür F, Tunçbilek G, Cila A. Evaluation of velopharyngeal insufficiency with magnetic resonance imaging and nasoendoscopy. Ann Plast Surg. 2000;44(1):8–13. [PubMed: 10651359]

Perry JL. Variations in velopharyngeal structures between upright and supine positions using upright magnetic resonance imaging. Cleft Palate Craniofac J. 2011;48:123–133. [PubMed: 20500077]

Perry JL, Kuehn DP, Sutton BP, Gamage JK. Anthropometric analysis of the velopharynx and related craniometric dimensions in three adult populations using MRI. Cleft Palate Craniofac J. 2014a, in press.

Perry JL, Kuehn DP, Sutton BP, Gamage JK. Sexual dimorphism of the levator veli palatini muscle: An imaging study. Cleft Palate Craniofac J. 2014b, 51(5):544–552. [PubMed: 23782419]

Perry JL, Kuehn DP, Sutton BP, Goldwasser MS, Jerez AD. Craniometric and velopharyngeal assessment of infants with and without cleft palate. J Craniofac Surg. 2011;22(2):499–503. [PubMed: 21403534]

Perry JL, Sutton BP, Kuehn DP, Gamage JK. Using MRI for assessing velopharyngeal structures and function. Cleft Palate Craniofac J. 2014c, 51(4): 476–485. [PubMed: 23566261]

Pigott RW. An analysis of the strengths and weaknesses of endoscopic and radiological investigations of the velopharyngeal incompetence based on 20 year experience of simultaneous recording. Br J Plast Surg. 2002;55:32–34. [PubMed: 11783966]

Price DL, De Wilde JP, Papadaki AM, Curran JS, Kitney RI. Investigation of acoustic noise on 15 MRI scanners from 0.2 T to 3 T. J Magn Reson Imaging. 2001;13:288–293. [PubMed: 11169836]

Sader R, Horch HH, Herzog M, Zeilhofer HF, Hannig C, Hess U, Bünte E, Böhme G. High-frequency videocinematography for the objective imaging of the velopharyngeal closure mechanism in cleft palate patients. Fortschr Kieferorthop. 1994;55:169–175. [PubMed: 7959485]

Sagar P, Nimkin K. Feasibility study to assess clinical applications of 3-T cine MRI coupled with synchronous audio recordings during speech in evaluation of velopharyngeal insufficiency in children. Pediatr Radiol. 2015;45(2):217–227. [PubMed: 25124806]

Scott AD, Boubertakh R, Birch MJ, Miquel ME. Towards clinical assessment of velopharyngeal closure using MRI: evaluation of real-time MRI sequences at 1.5 and 3T. Br J Radiol. 2012;85(1019):e1083–e1092. [PubMed: 22806623]

Scott AD, Wylezinska M, Birch MJ, Miquel ME. Speech MRI: morphology and function. Phys Med. 2014;30(6):604–618. [PubMed: 24880679]

Shinagawa H, Ono T, Honda EI, Masaki S, Shimada Y, Fujimoto I, Sasaki T, Iriki A, Ohyama K. Dynamic analysis of articulatory movement using magnetic resonance imaging movies: Methods and implications in cleft lip and palate. Cleft Palate Craniofac J. 2005;42(3):225–230. [PubMed: 15865454]

Silver AL, Nimkin K, Ashland JE, Ghosh SS, van der Kouwe AJ, Brigger MT, Hartnick CJ. Cine magnetic resonance imaging with simultaneous audio to evaluation pediatric velopharyngeal insufficiency. Arch Otolaryngol Head Neck Surg. 2011;137(3):258–263. [PubMed: 21422310]

Skolnick ML, Cohn ER. Videofluoroscopic Studies of Speech in Patients with Cleft Palate. New York: Springer-Verlag; 1989:1–48.

Suto Y, Matsuo T, Kato T, Hori I, Inoue Y, Ogawa S, Suzuki T, Yamada M, Ohta Y. Evaluation of the pharyngeal airway in patients with sleep apnea: value of ultrafast MRI imaging. AJF Am J Roentgenol. 1993;160:311–314.

Sutton BP. Fast, interative image reconstruction for MRI in the presence of field inhomegeneities. IEEE Trans Med Imaging. 2003:22:178–188. [PubMed: 12715994]

Sutton BP, Conway C, Bae Y, Brinegar C, Liang ZP, Kuehn DP. Dynamic imaging of speech and swallowing with MRI. Conf Proc IEEE Eng Med Biol Soc. 2009;6651–6654.

Sutton BP, Conway CA, Bae Y, Seethamraju R, Kuehn DP. Faster dynamic imaging of speech with field inhomogeneity correlated spiral fast low angle shot (FLASH) at 3T. J Magn Reson Imaging. 2010;32(5):1228–1237. [PubMed: 21031529]

Tian W, Li Y, Yin H, Zhao SF, Li S, Wang Y, Shi B. Magnetic resonance imaging assessment of velopharyngeal motion in Chinese children after primary palatal repair. J Craniofac Surg. 2010a;21(2):578–587. [PubMed: 20216434]

Tian W, Yin H, Li Y, Zhao S, Zheng Q, Shi B. Magnetic resonance imaging assessment of velopharyngeal structures in Chinese children after primary palatal repair. J Craniofac Surg. 2010b;21(2):568–577. [PubMed: 20216435]

Traser L, Burdumy M, Richter B, Vicari M, Echternach M. The effect of supine and upright position on vocal tract configuration during singing—a comparative study in professional tenors. J Voice. 2013;27(2):141–148. [PubMed: 23380394]

Vadodaria S, Goodacre TE, Anslow P. Does MRI contribute to the investigation of palatal function? Br J Plast Surg. 2000;53(3):191–199. [PubMed: 10738322]

Vorperian HK, Wang S, Schimek EM, Durtschi RB, Kent RD, Gentry LR, Chung MK. Developmental sexual dimorphism of the oral and pharyngeal portions of the vocal tract: an imaging study. J Speech Lang Hear Res. 2011;54(4):995–1010. [PubMed: 21106698]

Wylezinska M, Pinkstone M, Hay N, Scott AD, Birch BJ, Miquel ME. Impact of orthodontic appliances on the quality of craniofacial anatomical magnetic resonance imaging and real-time speech imaging. Eur J Orthod. 2015;in press

Williams RG, Preece M, Rhys R, Eccles R. The effect of adenoid and tonsil surgery on nasalance. Clin Otolaryngol Allied Sci. 1992;17(2):136–140. [PubMed: 1587028]

Wein BB, Drobnitzky M, Klajman S, Angerstein W. Evaluation of functional positions of tongue and soft palate with MR imaging: initial clinical results. J Magn Reson Imaging. 1991;1:381–383. [PubMed: 1802152]

Witzel MA, Stringer DA. Methods of assessing velopharyngeal function In: Bardach J, Morris HL, eds. Secondary Surgical Treatment of Cleft Palate. Philadelphia: WB Saunders; 1990:763–773.

Yamawaki Y, Nishimura Y, Suzuki Y. Rapid magnetic resonance imaging for assessment of velopharyngeal muscle movement on phonation. Am J Otolaryngol. 1997;18:210–213. [PubMed: 9164626]

Yildirim N, Fitzpatrick M, Whyte K, Jalleh R, Wightman A, Douglas N. The effect of posture on upper airway dimensions in normal subjects and in patients with the sleep apnea/hypopnea syndrome. Am Rev Respir Disord. 1991;144:845–847

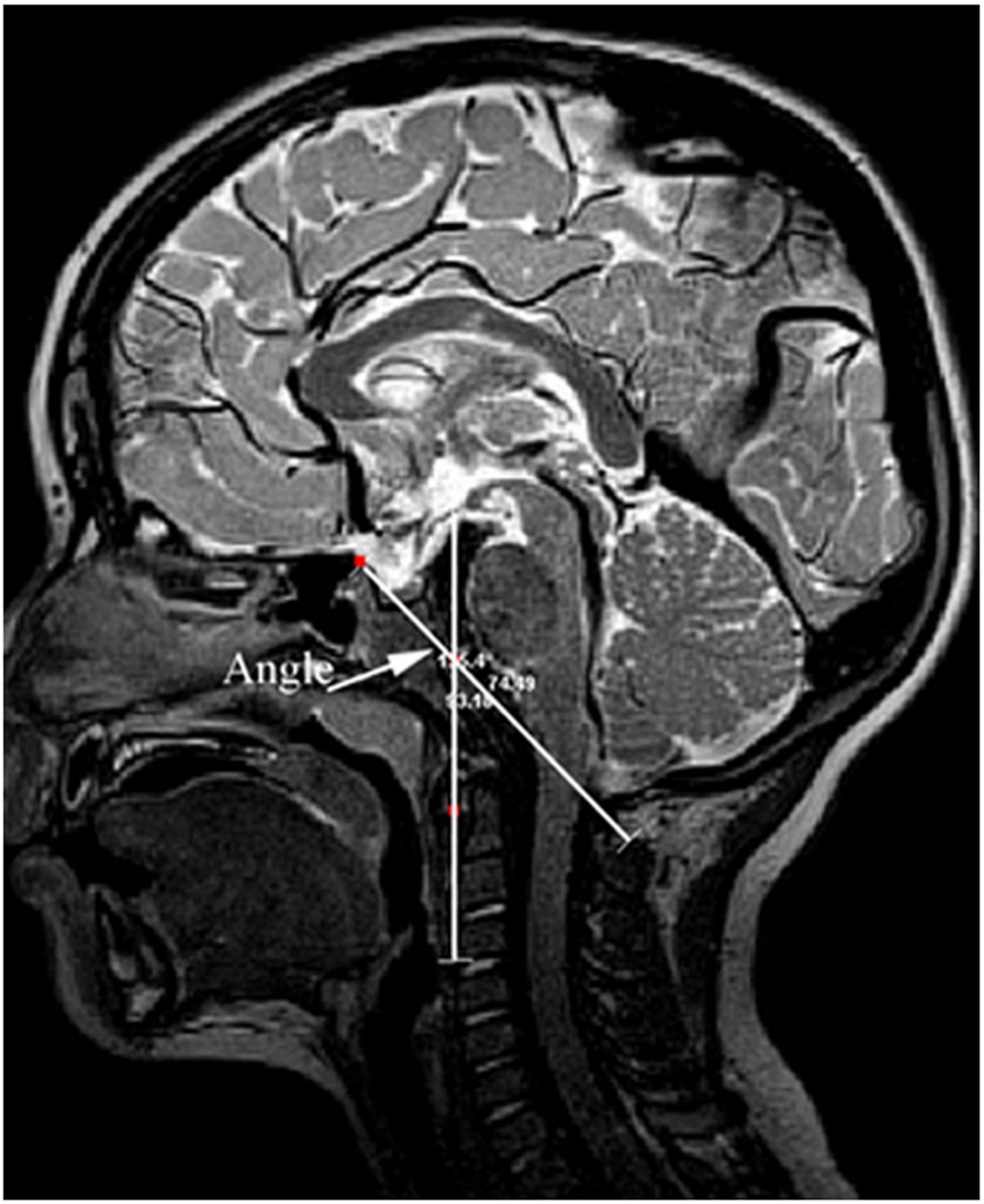

Figure 1:
Demonstration of measure for head flexion and extension. The vertical line passes along the anterior edge of the cervical vertebrae (C2-C3) and the oblique line connects the posterior tip of the spinous process of the first cervical vertebra with the tuberculum sella.

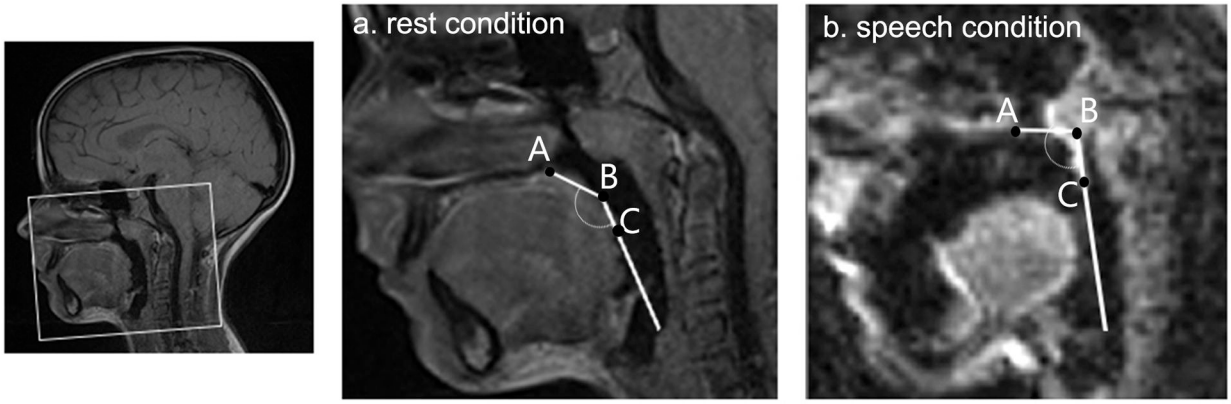

Figure 2:
Demonstration of the ABC angle obtained from midsagittal images at rest and during speech determined by intersecting points of posterior nasal spine (PNS), velar knee, and uvula. As the velar knee elevates the ABC angle decreases.

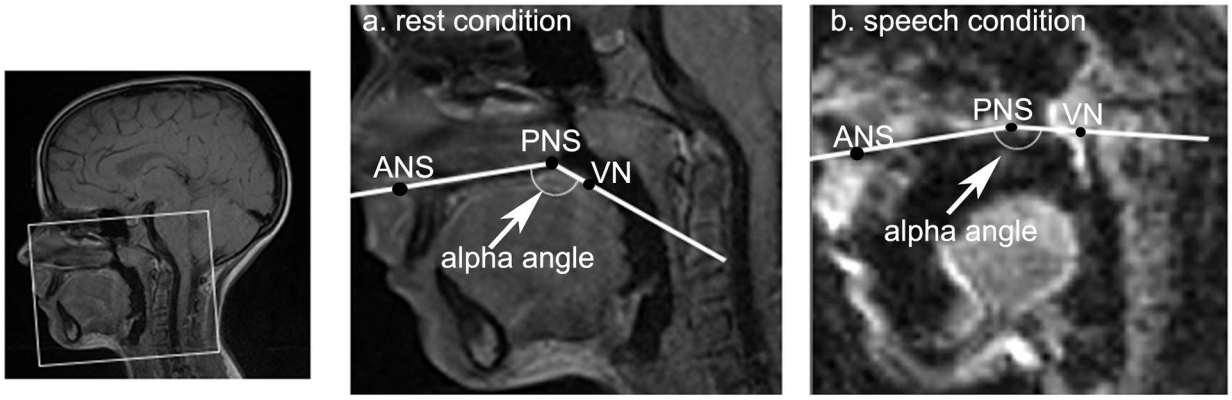

Figure 3:

Demonstration of the alpha angle obtained from midsagittal images determined by intersecting points of anterior nasal spine (ANS), posterior nasal spine (PNS), and velar knee (VN). Note as the velum elevates, the alpha angle becomes larger. An alpha angle of 180 degrees would indicate the velar knee was elevated to the level of palatal plane (ANS to PNS).

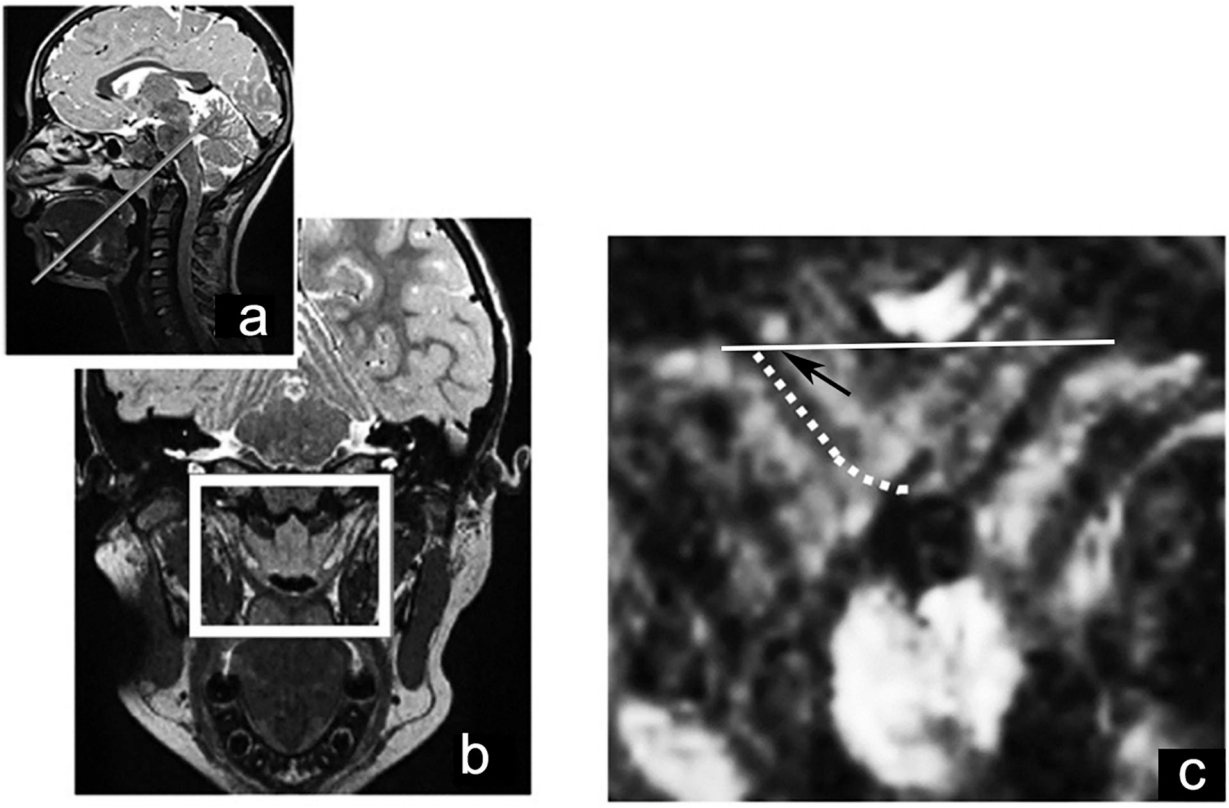

Figure 4:
The solid line (a) represents the image plane at which the oblique coronal image is obtained. The solid white box along the rest oblique coronal image (b) encompasses the levator muscle sling and is the field of view used in the dynamic oblique coronal images (c). The dotted white line (c) outlines the length of one levator muscle bundle and the arrow indicates the angle of origin. Note the dark muscle seen on the opposite side.

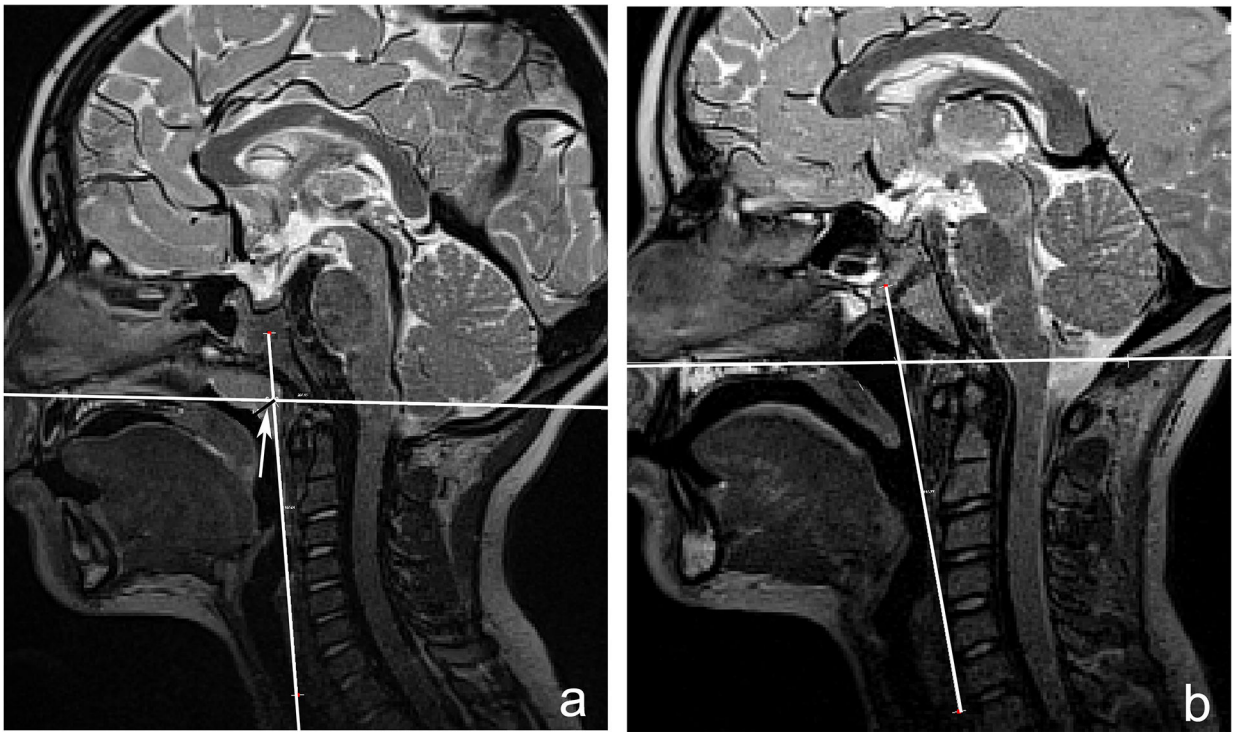

Fig 5:

Depth of the adenoid tissue was determined by measuring the nasopharyngeal margin of the adenoid tissue to the intersection of two reference lines—vertical line along the posterior pharyngeal wall and line through palatal plane (anterior nasal spine through posterior nasal spine). Image 5a presents a child with adenoid tissue and 5b presents a child with no apparent adenoid tissue.

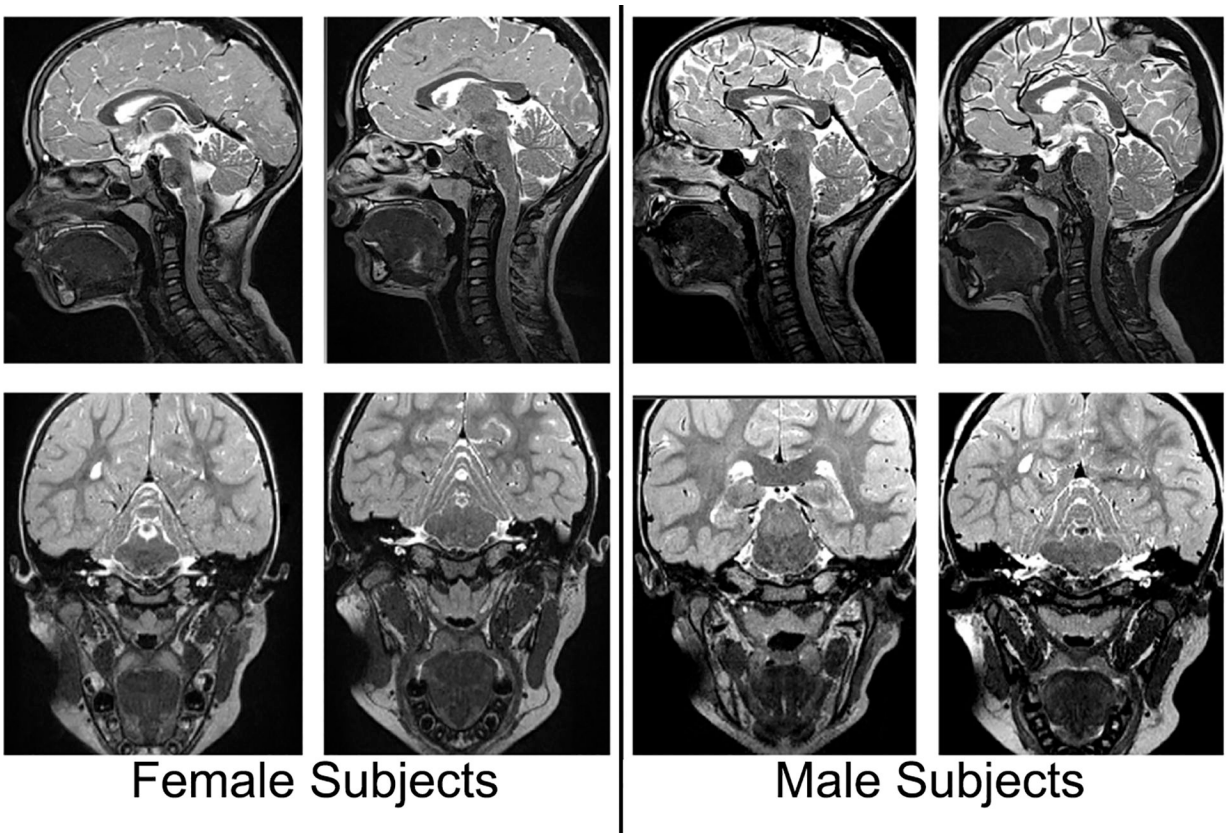

Figure 6.
Oblique coronal and midsagittal images at rest across the two randomly selected females and two randomly selected males.

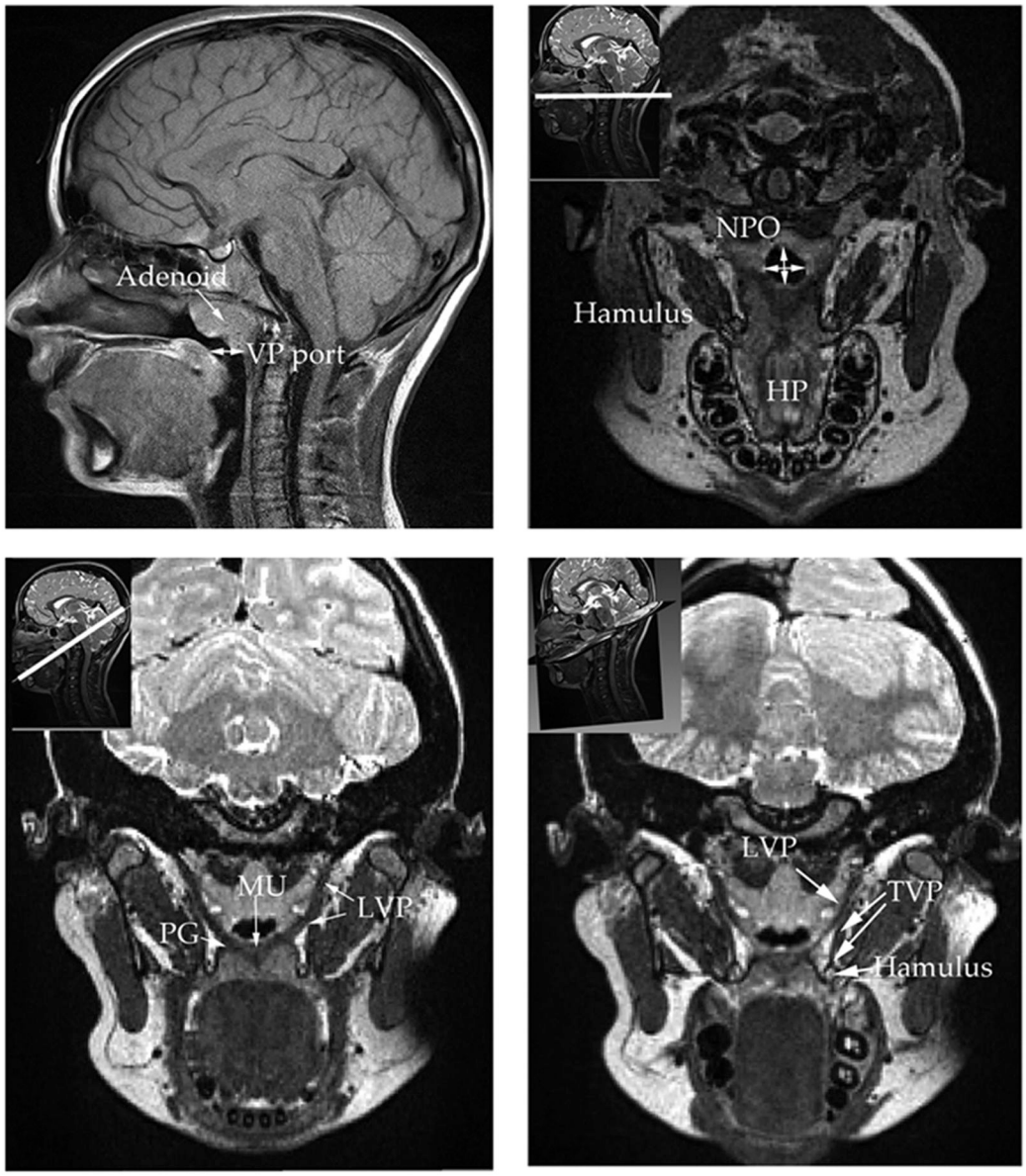

Figure 7:
Demonstration of the multiple viewpoints achieved using MRI to demonstrate sagittal (top left), axial (top right), oblique coronal (lower left), and an angled oblique coronal (lower right). As evident velar, velopharyngeal port (VP port), nasopharyngeal opening (NPO), cranial structures, hamulus, adenoids, musculus uvulae (MU), levator muscle (LVP), and palatoglossus (PG) can be visualized.

Table 1:

Subject demographics. All subjects were White native English speakers with clinically normal anatomy.

	Age (years)	Sex	Height (cm)	Weight (kg)
Child 01	7	Female	132	22
Child 02	5	Male	127	22
Child 03	8	Female	147	30
Child 04	9	Male	148	27
Child 05	6	Male	127	22
Child 06	5	Male	122	20
Child 07	9	Female	147	36
Child 08	7	Male	127	24
Child 09	5	Male	122	20
Child 10	4	Female	122	18
Child 11	9	Female	137	34
Mean (SD)	**6.7 (1.8)**	**---**	**132 (10.5)**	**25 (6)**

Table 2:

Magnetic Resonance Imaging (MRI) Protocol, 3 Tesla

	Static Three-Dimensional MRI Parameters	Dynamic MRI Parameters
Pulse sequence *	SPACE: T2 turbo spin echo. variable flip angle	FLASH: gradient echo sequence (GRE) six-shot spiral
Field of view	256 × 192 × 153.6 mm^3	240 × 240 × 8 mm^3
Repetition time	2500 ms	9 ms
Echo time	268 ms Echo train length: 171	Alternating between 1.3 and 1.8 ms
Resolution	0.8 mm isotropic	1.875 × 1.875 × 8 mm^3
Length of scan	4 minutes and 52 seconds for 1 static volume	50.5 seconds for 799 native frame rate images or 1515 sliding window images at 30 frames per second

* SPACE = sampling perfection with application optimized contrasts using different flip angle evolution; FLASH = Fast low-angle shot imaging.

Table 3:

Pearson Correlation and Mean Difference in Agreement Between Raters

	Pearson Correlation		Mean Difference in Agreement Between Raters
	Interrater	Intrarater	
ABC angle	0.98	0.98	2°
Alpha angle	0.65	0.78	1.4°
Levator muscle length	0.79	0.81	0.8 mm
Angle of levator muscle at origin	0.68	0.98	0.5°
Adenoid thickness	0.87	0.97	0.7 mm
Velar to adenoid depth	0.84	0.82	0.1 mm

Table 4:

Mean values and standard deviations in parentheses for rest and speech condition across the measures ABC angle (degrees), alpha angle (degrees), mean length of the right and left levator muscle bundles (mm), and angle or levator muscle origin at the base of the skull.

	Rest	**Speech**	**Paired T-test**
ABC Angle	142 (7)	80 (6)	$t_{(10)} = 85.903$, ***p* = .000****
Alpha angle	155 (10)	176 (4)	$t_{(10)} = -9.044$, ***p* = .000****
Levator muscle length	39.5 (2.9)	30.3 (4.4)	$t_{(10)} = 11.808$, ***p* = .000****
Angle of levator muscle at origin	56 (2)	46 (3)	$t_{(10)} = 11.9195$, ***p* = .000****
Adenoid thickness	4.7 (2.5)	--	--
Velar to adenoid depth	8.3 (1.9)	--	--

[+] Adenoid thickness and velar to adenoid depth are represented in mm and were obtained only from the midsagittal image at rest.

[*] $\alpha = 0.001$ significance level

Table 5:

Pearson correlation values for measures of the change (difference from rest to speech condition) for ABC angle, alpha angle, mean length of the right and left levator muscle bundle, and angle or levator muscle origin.

	ABC Angle	**Alpha Angle**	**Levator muscle**	**Angle of levator at origin**
ABC Angle	---	$r(11) = .680$ $\boldsymbol{p = .021}^{*}$	$r(11) = .685$ $\boldsymbol{p = .020}^{*}$	$r(11) = .399$ $p = .224$
Alpha Angle	$r(11) = .680$ $\boldsymbol{p = .021}^{*}$	---	$r(11) = .703$ $\boldsymbol{p = .016}^{*}$	$r(11) = .433$ $p = .184$
Levator muscle length	$r(11) = .685$ $\boldsymbol{p = .020}^{*}$	$r(11) = .703$ $\boldsymbol{p = .016}^{*}$	---	$r(11) = .814$ $\boldsymbol{p = .002}^{*}$

$^{*}\alpha = 0.05$ significance level; (n=11)

Table 6:

Pearson correlation values for comparisons of adenoid and velar to adenoid depth to measures of the change between speech and rest for ABC angle, alpha angle, mean length of the right and left levator muscle bundle, and angle or levator muscle origin.

	Adenoid thickness	Velar to adenoid depth
ABC Angle	$r(11) = -.404$, $p = .218$	$r(11) = -.357$, $p = .281$
Alpha Angle	$r(11) = -.391$, $p = .234$	$r(11) = -.362$, $p = .275$
Levator Muscle	$r(11) = -.660$, $\mathbf{p = .027}^{*}$	$r(11) = .165$, $p = .628$
Angle of origin	$r(11) = -.770$, $\mathbf{p = .006}^{*}$	$r(11) = .369$, $p = .264$

$^{*}\alpha = 0.05$ significance level